HVAC&R Research

Publication details, including instructions for authors and subscription information:
http://www.tandfonline.com/loi/uhvc20

Air bypass in vertical stack water source heat pumps

Kapil Varshney [a], Ian Shapiro [a], Yossi Bronsnick [a] & Jim Holahan [a]

[a] Taitem Engineering, Ithaca, NY, 14850, USA

Available online: 03 Oct 2011

To cite this article: Kapil Varshney, Ian Shapiro, Yossi Bronsnick & Jim Holahan (2011): Air bypass in vertical stack water source heat pumps, HVAC&R Research, 17:5, 692-709

To link to this article: http://dx.doi.org/10.1080/10789669.2011.585683

Taylor & Francis
Taylor & Francis Group

Air bypass in vertical stack water source heat pumps

Kapil Varshney,* Ian Shapiro, Yossi Bronsnick, and Jim Holahan
Taitem Engineering, Ithaca, NY 14850, USA
**Corresponding author e-mail: kvarshney@taitem.com*

Vertical stack water source heat pumps are widely used to provide both comfort cooling and heating to buildings. A problem of air bypass, in which some return air does not pass over the indoor coil of the heat pump, was encountered, causing performance degradation of the heat pumps. This article quantifies the air bypass problem in vertical stack water source heat pumps and the associated impacts. Field testing at five different sites was performed, and results show that air bypass occurred in all five installations. Three methods are proposed to detect and diagnose the air bypass problem. By sealing air bypass locations after the diagnostics, the improvement in cooling efficiency ranged from ∼7% to 17% and averaged 12.8%, and the improvement in heating efficiency ranged from ∼16% to 19% and averaged 17.5%. Based on the locations of air bypass, it is shown that ∼55% of bypassed air was passing through the locations, which are common in all types of heat pumps.

Introduction

Approximately 14% of the total energy and 32% of the electricity generated in the United States are consumed by HVAC systems to meet the heating and cooling demands of residential and commercial buildings (DOE 2003; ASHRAE 2003). Among all HVAC systems, water source heat pumps (WSHPs) in particular are increasingly popular, especially in high-performance buildings. According to the U.S. census bureau, shipments of WSHPs rose 40% from 2005 to 2006, for example, while industry-wide HVAC equipment shipments of all types rose only 3% (U.S. Census Bureau 2006).

Many HVAC systems fail to match the performance criteria envisioned at design. A study performed by Proctor (2004) in the United States of over 55,000 air-conditioning units showed that more than 90% were operating with one or more kinds of faults. Another study of over 13,000 air-conditioning units showed that 57% of the systems were either undercharged or overcharged for refrigerant, causing them to operate below their designed efficiency (Downey and Proctor 2002). In a survey, over 1400 rooftop units were studied, and the results showed that the average operating efficiency of the units was 80% of designed performance (Rossi 2004). A modeling study performed on air-conditioning units showed that increases in supply- and return-duct leakage from 0% to 11% decreased cooling capacity by 34%, and the combined effects of a 30% undercharged unit with 30% duct leakage decreased the capacity over 50% (Walker et al. 1998).

Several fault detection and diagnostic (FDD) methods have been proposed that detect and diagnose faults and their causes at an early stage in order to prevent additional damage and energy waste. Fault detection is a process to determine the faults in an HVAC system, whereas fault diagnostics involve

Received January 5, 2011; accepted April 21, 2011
Kapil Varshney, PhD, Member ASHRAE, is Research Department Manager. **Ian Shapiro, PE**, Member ASHRAE, is President. **Yossi Bronsnick** is Structural Engineer. **Jim Holahan** is Energy Analyst.

HVAC&R Research, 17(5):692–709, 2011.
ISSN: 1078-9669 print / 1938-5587 online
DOI: 10.1080/10789669.2011.585683

reasons of a fault and its identification. Katipamula and Brambley (2005a, 2005b) provided an extensive review in the FDD area to identify different technologies that are suitable for building HVAC systems over the past decades. In addition, artificial neural network (ANN) capability has widely been used not only for controlling HVAC equipment, but for fault diagnosis by many researchers (Diaz et al. 2001; Varshney and Panigrahi 2005). Li and Braun (2003) developed a practical automated FDD technique with the capability to handle multiple simultaneous faults and implemented a polynomial neural network regression in their reference model. Navarro-Esbri et al. (2007) developed a fault-detection tool based on a neural network for a water-to-water vapor compression system with a particular emphasis on refrigerant leak detection. Wang and Wang (1999), Wang and Xiao (2004), and Lee et al. (2005) presented the sensor FDD methods applicable for HVAC systems. Other FDD methods to detect and diagnose faults in various HVAC systems can be found in Grimmelius et al. (1995), Dexter and Benorarets (1996), Dexter and Ngo (2001), Kelso and Wright (2005), and Reddy (2007).

Though FDD is widely used to improve the performance of HVAC systems, the accuracy and reliability of FDD methods depend on the reliability of the sensor measurements. In addition, FDD models and standard commissioning tests, such as measurement of supply airflow, measurement of the refrigerant pressure of the system, and thermostat response tests, might not identify air bypass. The literature survey indicates that air-bypass in WSHP systems does not appear to have previously been identified as an issue. This article presents the impact of air bypass on the performance of vertical stack WSHPs (VSWSHP) and proposes three methods to identify air bypass. Field testing was performed at five different sites where the VSWSHP systems were installed, and locations of air bypass were identified. Hereafter in this article, heat pump will be used in lieu of VSWSHP.

Fault description

Air bypass is a problem in which some return air does not pass over the indoor coil of a heat pump. A fraction of the return air is pulled into the cabinet through gaps and holes, such as through piping penetrations behind the heat pump, through the heat pump front panel, and at junctions where the heat pump is supposed to seal with the equipment cabinet as it slides in.

There are several impacts of air bypass on the performance of heat pumps. Immediate impacts of air bypass are:

- low suction pressure in cooling, and
- high condensing pressure in heating.

End impacts of air bypass are:

- vulnerability to freeze-up in cooling,
- vulnerability to high-pressure trip in heating, and
- low efficiency in heating and cooling.

Most dramatically, if a heat pump is running in the cooling mode, the indoor coil might freeze and the heat pump can stop working (Figure 1). When the surface of the indoor coil drops below 32°F (0°C), ice formation is likely on that surface. As is shown in Figure 1, due to the air bypass problem, a solid block of ice was formed over the indoor coil of a heat pump within an hour of startup. Figure 2 shows the variation of return air temperature (T_{in}), air temperature leaving the indoor coil (T_C), and supply air temperature (T_{out}) over time. It can be noted in the graph that the air temperature leaving the indoor coil rapidly dropped below 32°F (0°C) and continued to decrease, which caused ice formation over the indoor coil. Figure 3 shows the variations of T_{in}, T_C, and T_{out} after blocking air bypass, and it can be noted that after preventing the air bypass, the temperature of air leaving the coil (T_C) stayed above 32°F (0°C).

Details of field experiments

Field experiments were executed during 2009 and 2010 in five buildings to investigate the air bypass problem in heat pumps. A typical schematic of a heat pump is presented in Figure 4. The water-to-air heat pumps typically consist of an aluminum fin and copper tube heat exchanger on the air side, double-tube heat exchanger with an inner convoluted tube and the refrigerant flowing in the annular space on the water side, a hermetic compressor, thermostatic expansion valve, a reversing valve, and a control system.

The heat pumps investigated in this study had total cooling capacities between ~1.5 tons (5.2 kW) and 3.5 tons (12 kW). Field test conditions for all five sites are presented in Table 1. All of the heat pumps were fairly new, installed within

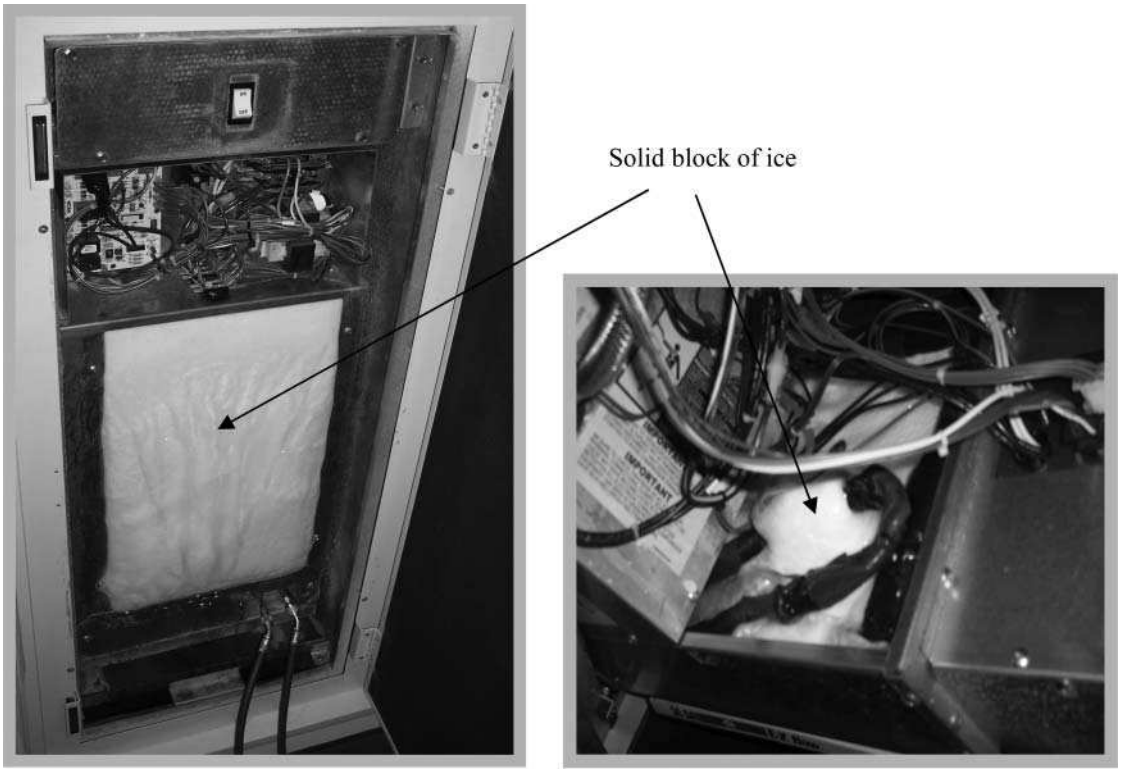

Figure 1. Solid block of ice over indoor coil.

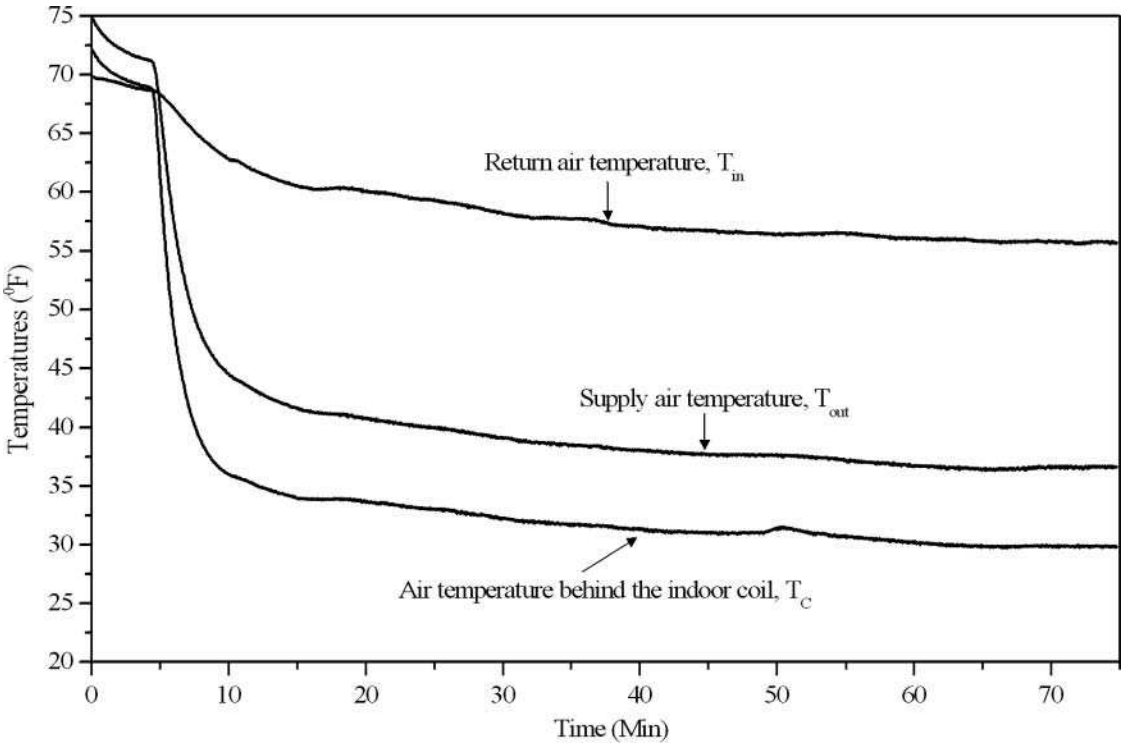

Figure 2. Temperature variation of supply air, return air, and air behind the coil before sealing.

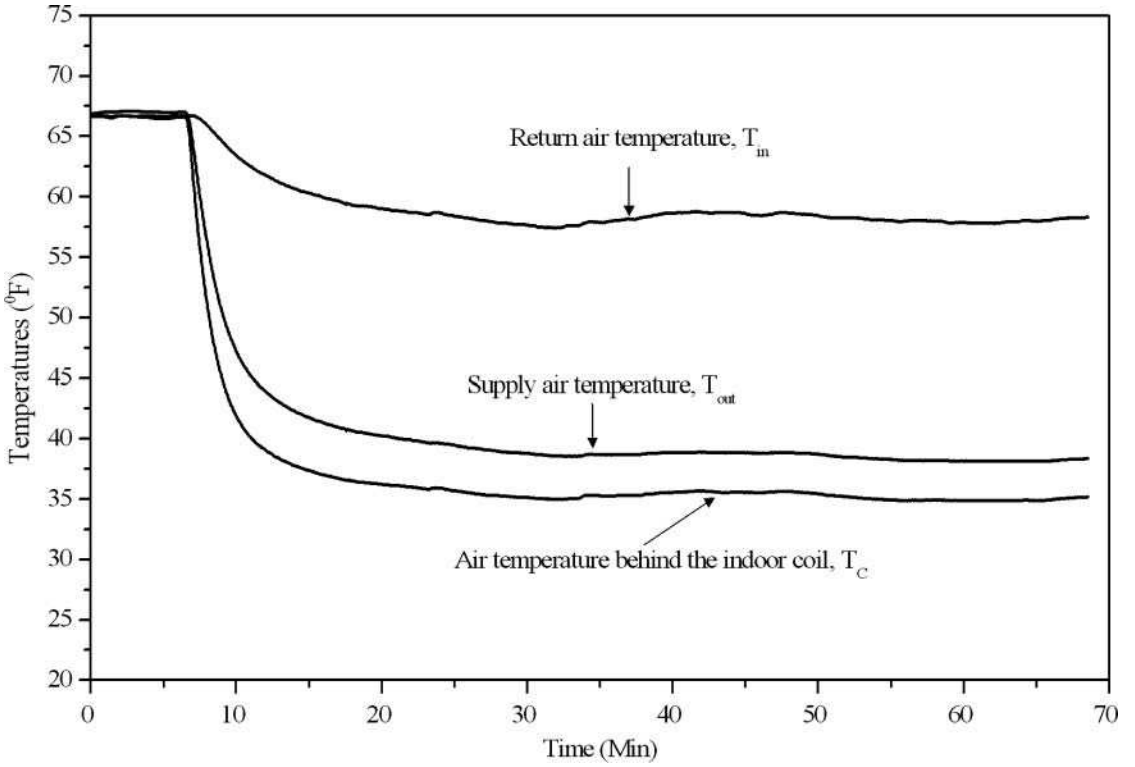

Figure 3. Temperature variation of supply air, return air, and air behind the coil after sealing.

the past three years by three different major heat pump manufacturers. Each heat pump unit had a user-controlled thermostat to maintain the indoor air temperature at a desired set-point. Thermostats were located on the wall about 5 ft (1.5 m) off the floor. Heated or cooled air was delivered to the designated areas through supply ducts with wall- or ceiling-mounted supply registers. Return air entered into the unit by passing around the access door on front of the unit. The heat pumps were located inside of a drywall enclosure. Inside of the enclosure, there was a sheet metal cabinet in which the chassis was

Table 1. Field test conditions at sites.

Parameters	Site 1	Site 2	Site 2	Site 4	Site 5
Entering Water Treatment, °F (°C)	81 (27.2)	60 (15.6)	70 (21.1)	66 (18.9)	89 (31.7)
Indoor-air temperature					
Baseline, °F (°C)	73 (22.8)	74 (23.3)	73 (22.8)	72 (22.2)	71 (21.7)
After sealing, °F (°C)	76 (24.4)	72 (22.2)	74 (23.3)	76 (24.4)	68 (20.0)
Indoor-air relative humidity					
Baseline,%	58	25	58	27	49
After sealing,%	53	29	72	29	56
Outdoor-air temperature					
Baseline, °F (°C)	31 (−0.6)	44 (6.7)	49 (9.4)	31 (−0.6)	79 (26.1)
After sealing, °F (°C)	30 (−1.1)	45 (7.2)	41 (5.0)	53 (11.7)	89 (31.7)
Outdoor-air relative humidity					
Baseline,%	49	71	36	36	71
After sealing,%	51	81	19	47	57

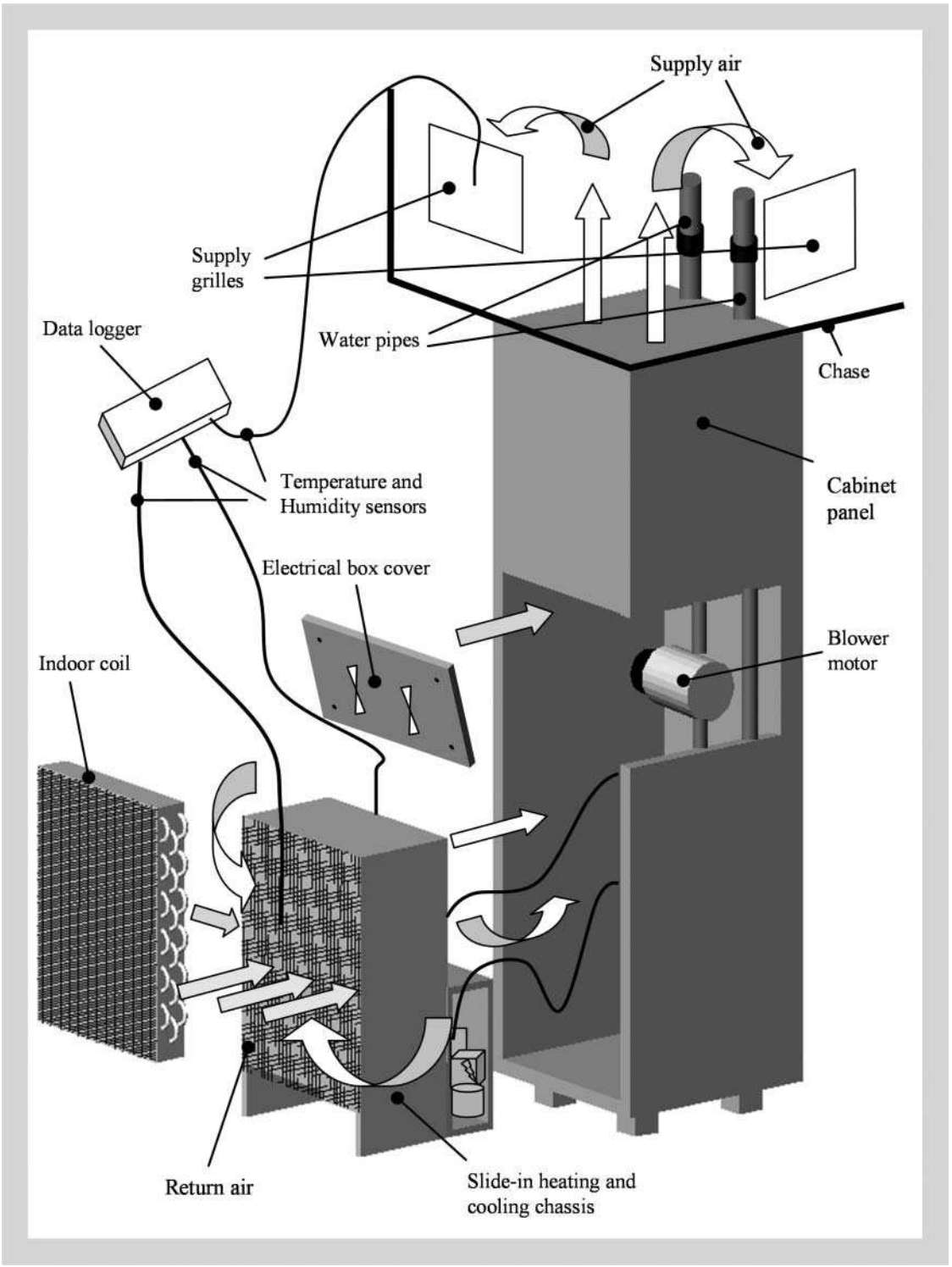

Figure 4. Schematic of a VSWSHP and test instrumentation.

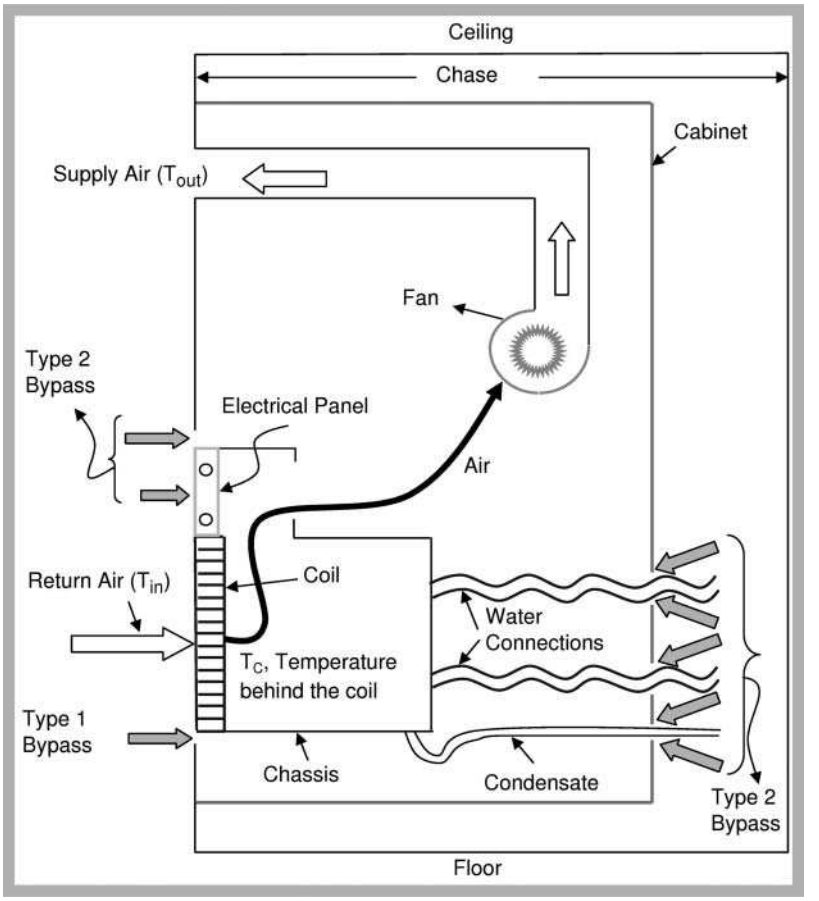

Figure 5. Potential locations of air bypass in a VSWSHP.

located. The cabinet and the chassis were manufactured products, while the drywall assembly was site built. The heat pumps were mounted in the drywall chase, and the interior of the sheet metal cabinet was covered with insulation. Water pipes were typically copper and entered the unit from the rear.

As mentioned before, only VSWSHPs have been selected in this investigation. These heat pumps can be divided in two main parts—a cabinet typically comprised of a sheet metal housing and a blower section, and a chassis containing the full refrigeration circuit that slides into the cabinet. Based on the locations of air bypass, the sources of air bypass can broadly be divided in two types. Type 1 is the locations that can only be found in VSWSHPs, such as the junction where the sliding heat pump chassis is supposed to seal with the cabinet as it slides in; type 2 is the locations that are common to all types of WSHPs. These locations of air bypass are water pipe penetrations, condensate pipe penetrations, cabinet seams, electrical connections, control connections, etc. (Figure 5).

Initially, the locations of air bypass in the heat pumps were identified at each site by using the smoke flow visualization technique and were sealed one by one. Visual inspection and smoke testing were also performed before and after each sealing. This allowed an assessment of the quality of air-sealing before moving on to each subsequent test. For all tests, the relative quantities of air bypass were disaggregated for the different types of bypass. This disaggregation was done through repeated measurement of air bypass after each type of hole was sealed and visually inspected.

A balometer was used to measure volumetric airflow rates of total return air to the heat pump, total supply air, and air entering the indoor coil. A portable data logger, in conjunction with four temperature and relative humidity sensors, was used to measure the dry-bulb temperatures and

relative humidity of the return air, the air leaving the indoor coil, the supply air, and the ambient air. Temperatures and relative humidity data were sampled at 1-sec intervals. In order to calculate the efficiency (energy efficiency ratio [EER] in cooling or coefficient of performance [COP] in heating) of the heat pump, instantaneous power across the main power supply terminals inside the electrical panel of the heat pump was measured. A power transducer in conjunction with a data logger was used to measure the power consumption of the heat pump.

Methodology

In order to diagnose the air bypass problem, three different methods have been employed: volumetric airflow tests (direct measurement of airflow), an air temperature mixing test, and a blocked coil method. Visual inspection and smoke testing were performed before measurements were taken and again after each incremental improvement to assure proper sealing. In particular, visible holes into the chase or areas where dust had accumulated as an indication of bypass were found. Three methods were used to evaluate air bypass.

1. **Balometer airflow testing method.** A series of balometer tests were performed on the heat pump units. These included a baseline test (before sealing), followed by a series of tests to measure the effect of incremental sealing aimed at reducing bypass. In each test, a balometer was used to measure the total supply airflow, total return airflow, and the airflow just across the indoor coil (plate fin heat exchanger). This allowed the separation of air bypass associated with the face of the unit and air bypass occurring in other parts of the cabinet.
2. **Air temperature method.** Air temperature mixing tests were taken by placing temperature and relative humidity probes in front of the indoor coil to measure the temperature and relative humidity of the return air, air properties of the air leaving the indoor coil, and temperature and relative humidity of the supply air. The variables are shown in Figure 5. Data were recorded continuously throughout the process and results were obtained after each air-sealing. Based on the following calculation, the fraction of air bypass was estimated:

$$\text{Air bypass} = \frac{T_{out} - T_C}{T_{in} - T_C} \times V, \qquad (1)$$

where V (ft^3/min or m^3/min) was the volumetric flow rate at the supply grille. The appendix provides a detailed derivation of this equation with all the assumptions considered to derive it.

3. **Blocked coil method.** This approach was also used to examine air bypass. In this method, the return air on the front face of the indoor coil was blocked, and the volumetric airflow at the supply grille was measured, which essentially represented all bypasses, as no airflow was being allowed through the coil. Since the coil was blocked, the blower would be operating at a higher pressure. As a result, this measurement was less accurate than the other two methods.

The combination of these three methods allowed verification of results by checking the data from each method against the others.

Uncertainty analysis

Uncertainty analysis is required to indicate the accuracy of the experiments. An uncertainty analysis was performed using the method described by Holman (2001), which states

$$e_Y^2 = \left(\frac{\partial Y}{\partial X_1}\right)^2 e_{X_1}^2 + \left(\frac{\partial Y}{\partial X_2}\right)^2 e_{X_2}^2 + \ldots\ldots\ldots\ldots + \left(\frac{\partial Y}{\partial X_J}\right)^2 e_{X_J}^2, \qquad (2)$$

where e_Y represents the overall uncertainty, Y is the calculated results, $Y = Y(X_1, X_2, \ldots, X_J)$, and $e_{X1,\ldots,J}$ represents the individual uncertainties in the variables $x_{1,\ldots,j}$. The instrumentation ranges and their uncertainties are presented in Table 2. In the present study, the temperatures, relative humidity, flow rates, and instantaneous power were measured with the instruments described above. Total cooling capacity (TCC), latent cooling capacity (LCC), sensible cooling capacity (SCC), sensible heat ratio (SHR), EER, total heating capacity (THC), and COP were calculated using equations given below.

$$\text{TCC} = \frac{60 \times V \times (h_{in} - h_{out})}{\nu \times (1 + W_{out})}, \qquad (3)$$

$$\text{LCC} = \frac{60 \times 1060 \times V \times (W_{in} - W_{out})}{\nu \times (1 + W_{out})}, \qquad (4)$$

$$\text{SCC} = \frac{60 \times V \times c_{pa} \times (T_{in} - T_{out})}{\nu \times (1 + W_{out})}. \qquad (5)$$

Table 2. Instrumentation range and uncertainty.

Instrument	Range	Uncertainty
1. Balometer	50–1200 CFM	±3.000%
2. Temperature sensor	32–122°F (0–°C)	±0.380°F (±0.211°C)
3. Relative humidity sensor	10–90%	±2.500%
4. kWHr transducer	0 to 100 kW	±1.000%

The SHR is defined as the ratio of the SCC to the TCC,

$$\mathrm{SHR} = \frac{\mathrm{SCC}}{\mathrm{TCC}} \tag{6}$$

The EER of the heat pump is defined as

$$\mathrm{EER} = \frac{3.412 \times TCC}{P_{hp}} \tag{7}$$

The THC was obtained using the following equation:

$$\mathrm{THC} = 1.08 \times V \times (T_{\mathrm{out}} - T_{\mathrm{in}}), \tag{8}$$

and the COP of the heat pump was obtained using the following equation:

$$\mathrm{COP} = \frac{\mathrm{THC}}{\mathrm{P}_{hp}} \tag{9}$$

The total uncertainties of the measurements are estimated to be ±0.380°F for the temperatures, ±2.500% for the relative humidity, ±3.000% for flow rates, and ±1.000% for instantaneous power of the heat pump.

The uncertainties of the TCC, efficiency (in cooling mode, EER), THC, and efficiency (in heating mode, COP) for all sites were calculated on the basis of measured uncertainties of temperature, relative humidity, heat pump power, and volumetric flow rates (Table 3):

$$TCC = f(T_{in}, T_{out}, RH_{in}, RH_{out}, V) \tag{10}$$

Table 3. Relative uncertainties for TCC, THC, EER, and COP.

	Parameter	Uncertainty
Cooling mode	TCC	±5.362% to ±10.808%
	EER	±5.933% to ±10.857%
Heating mode	THC	±3.456% to ±4.221%
	COP	±8.912% to ±14.179%

and

$$\mathrm{EER} = f(T_{in}, T_{out}, RH_{in}, RH_{out}, V, P_{hp}), \tag{11}$$

$$\mathrm{THC} = f(T_{in}, T_{out}, V), \tag{12}$$

and

$$\mathrm{COP} = f(T_{in}, T_{out}, V, P_{hp}). \tag{13}$$

RH_{in} and RH_{out} are the relative humidity of the return and supply air, respectively. In the uncertainty calculations on the EER and COP, the uncertainty due to entering water temperature (EWT) is neglected.

It is also noted that the uncertainty discussed above is limited to the operation ranges of return and supply air temperatures, return and supply air relative humidity, and volumetric flow rate at the supply grille. If the temperatures, relative humidities, and volumetric flow rate are considerably away from the test conditions mentioned in Table 1, the uncertainties of the parameters presented in Table 3 are expected to be different. In addition, both TCC and THC are dependent on some of the test conditions, such as T_{in}, EWT, entering wet-bulb temperature (EWB), and V. For a given site, EWT was approximately constant before and after the sealing. However on the sites, T_{in} and RH_{in} varied slightly before and after the sealing (Table 1). While calculating the TCC, THC, EER, and COP of the heat pumps, instantaneous test conditions were considered. Nevertheless, due to the difference in test conditions (T_{in}, RH_{in}, etc.) before and after the sealing, their effects on the improvements of measured parameters (TCC, THC, EER, etc.) are neglected in the subsequent analysis.

Results and discussion

Extensive testing at each site was done; however, for brevity, only the data collected at the fifth site will be discussed. Summary results are presented for all five sites.

Cooling calculations

Readings were taken when the unit was running in cooling mode with a set-point temperature of 66.200°F (19.000°C). After several minutes of testing, temperature and relative humidity were recorded along with the unit's power consumption. Power readings were used for the efficiency calculations when the return air temperature was 66.800°F (19.333°C). The indoor air enthalpy method has been used in this study to calculate the TCC of the heat pumps. The performance of the heat pumps was studied by measuring the airflow rates (supply and return), temperatures of supply and return air, temperature leaving the indoor coil, and total power consumption when the heat pump was running. The heat pump unit was allowed to run long enough so that it could come to a quasi-steady state.

A baseline measurement to determine the air bypass was performed before sealing air bypass locations. After taking these baseline readings, a series of measurements to determine the reduction in air leakage as a result of incremental improvements was performed. After each air-sealing step, a smoke test was conducted to ensure that the sealing of the target area was complete. There were four general locations of air bypass found (Table 4). The baseline balometer test showed that the supply airflow was 675 ft^3/min (19.114 m^3/min), and the return flow over the coil was 513 ft^3/min (14.527 m^3/min). The balometer test was repeated after each air-sealing step. Once the measurements were taken for each air-sealing step, the reduction in air bypass for each location was determined. Table 4 presents the supply airflow, airflow over the indoor coil and reduction in air bypass after sealing each location, and uncertainties associated with the measurements.

Table 5 presents the reduction in air bypass using the air-mixing method. Equation 1 is used to calculate reduction in air bypass, and Equation 2 is used to calculate uncertainty in the reduction in air bypass (Table 5). It can be seen in Tables 4 and 5 that both methods showed similar reduction in air bypass after sealing all locations of air bypass. It can also be noted in Table 4 that after sealing the final location of air bypass, there is still a significant difference in total supply airflow and the airflow over the indoor coil. This results from the fact that the unit was located in a drywall chase and the interior of the sheet metal cabinet was covered with insulation so that not all parts of the sheet metal cabinet could be inspected or accessed for sealing.

The reduction in air bypass using the blocked coil method is presented in Table 6. As discussed above, the reduction in air bypass after all sealing when using the blocked coil method is higher than the reduction in air bypass obtained using the two other methods. The blocked coil method is expected to give exaggerated results, because blocking the coil itself affects air pressures throughout the system. Therefore, uncertainty analysis for this method is not presented. Though the blocked coil method is likely less accurate, it remains useful because it can be employed as a quick commissioning test. If the air is not bypassing the coil, there will be no airflow at the supply after blocking the indoor coil.

Throughout the tests, some unexpected results are noted. For example, the blocked coil tests show lower air bypass after the first one or two steps of air-sealing when higher air bypass would be expected compared to the other two methods. In general, taking measurements under field conditions proved challenging. Balometers themselves have an accuracy of 3%, even when calibrated; beyond that, they can show readings that fluctuate by several CFM within a given test due to airflow turbulence. Sealing the balometer at its edges around the surface against which it is mating can be difficult. Temperature measurements for the air temperature mixing method are ostensibly affected by radiation from nearby cold and hot surfaces (for example, the coil itself). Table 7 shows significant improvement in the efficiency (EER) of the heat pump after each sealing step. Based on the uncertainty analysis for EER presented in Table 7, a range from 4.696% to 24.038% and averaged 14.367% improvement in cooling efficiency was obtained.

Heating calculations

A similar approach was considered to examine the effect of air bypass on the performance of the heat pump when it was running in heating mode.

Table 8 presents the efficiency of the heat pump before and after all air-sealing. Based on uncertainty analysis for COP presented in Table 8, a range from 6.581% to 31.633% and averaged 19.107% improvement in COP efficiency was obtained after sealing all accessible locations of air bypass.

Table 4. Airflow measurements using balometer (site 5).

	Total supply airflow		Airflow over the indoor air coil		Reduction in air bypass	
Order of sealing	ft^3/min	m^3/min	ft^3/min	m^3/min	ft^3/min	m^3/min
1. Baseline measurement	675 ± 20.254	19.114 ± 0.574	513 ± 15.386	14.527 ± 0.436	N.A.	N.A.
2. Holes at the top panel and the open cell foam gasket between the cabinet and the face panel	666 ± 19.981	18.859 ± 0.566	527 ± 15.814	14.923 ± 0.448	0–36.074	0–1.022
3. Gaps around the edges of the front panel and bottom left corner	665 ± 19.954	18.831 ± 0.565	531 ± 15.927	15.036 ± 0.448	0–40.157	0–1.137
4. Gaps around the indoor coil	675 ± 20.254	19.114 ± 0.574	550 ± 16.504	15.574 ± 0.467	14.437–59.563	0.408–1.687
5. Pipe penetration through the rear of the cabinet	678 ± 20.342	19.199 ± 0.576	570 ± 17.104	16.141 ± 0.484	33.986–80.023	0.962–2.266

Table 5. Reduction in air bypass using air temperature mixing method (site 5).

Order of sealing	Reduction in air bypass	
	ft^3/min	m^3/min
1. Holes at the top panel and open cell foam gasket between the cabinet and the face panel	0–54.265	0–1.536
2. Gaps around the edges of the front panel and bottom left corner	0–58.407	0–1.654
3. Gaps around the indoor coil	15.333–67.162	0.434–1.902
4. Pipe penetrations through the rear of the cabinet	34.858–82.601	0.987–2.339

Psychrometric analysis (cooling mode)

Figure 6 shows a psychrometric representation of the air bypass problem in cooling mode. Three statepoints in the unit were analyzed. State points 1′, 2′, and 3′ represent the air properties of return air, air leaving the indoor coil, and supply air, respectively, when a fraction of the air was bypassing the indoor coil. State points 1, 2 and 3 represent the air properties of return air, air leaving the indoor coil, and supply air, respectively, when the possible areas of air bypass were sealed. The analysis presented below at these state points is based on the data collected for a typical warm day with the heat pump running in cooling mode. In both cases, before and after the sealing, ambient air temperature was set at 66.200°F (19.000°C) using a manually controlled thermostat. The design loads of the heat pump are 1.670 tons (5.873 kW) for the total cooling load, 1.270 tons (4.466 kW) for the sensible load, and 0.400 tons (1.407 kW) for the latent load. The design volumetric flow rate of the unit was 630 ft^3/min (17.840 m^3/min). The design efficiency of the heat pump in cooling mode (EER) was 17.200 and in heating mode (COP) was 4.400.

Psychrometric analysis before sealing

State point 1′ represents the return air conditions in steady state. A sensor is used to measure the temperature and relative humidity of the return air, which were T_{in} = 66.860°F (19.367°C) and RH_{in} = 52.480% with a corresponding humidity ratio of W_{in} = 0.007359 $lb_{water}/lb_{dry\text{-}air}$ ($kg_{water}/kg_{dry\text{-}air}$). Total enthalpy associated to the return ambient air to the unit was 24.195 Btu/lb (56.278 kJ/kg). The volumetric airflow rate was 675 ft^3/min (19.114 m^3/min). State point 2′ represents the temperature and relative humidity of the air leaving the indoor coil. The temperature and relative humidity at 2′ were 44.200°F (6.778°C) and 91.490%, respectively, with a corresponding humidity ratio of W_C = 0.005592 $lb_{water}/lb_{dry\text{-}air}$ ($kg_{water}/kg_{dry\text{-}air}$). The total enthalpy associated with the air leaving the indoor coil was 16.735 Btu/lb (38.926 kJ/kg). State point 3′ represents the supply air conditions. The temperature and relative humidity of the supply air were 49.460°F (9.700°C) and 80.580%, respectively, with a corresponding humidity ratio of W_{out} = 0.006012 $lb_{water}/lb_{dry\text{-}air}$ ($kg_{water}/kg_{dry\text{-}air}$). Total enthalpy associated to the supply air was 18.464 Btu/lb (42.947 kJ/kg).

Table 6. Reduction in air bypass using blocked coil method (site 5).

Order of sealing	Reduction in air bypass	
	ft^3/min	m^3/min
1. Holes at the top panel and the open cell foam gasket between the cabinet and the face panel	6	0.170
2. Gaps around the edges of the front panel and bottom left corner	20	0.566
3. Gaps around the indoor coil	35	0.991
4. Pipe penetrations through the rear of the cabinet	90	2.549

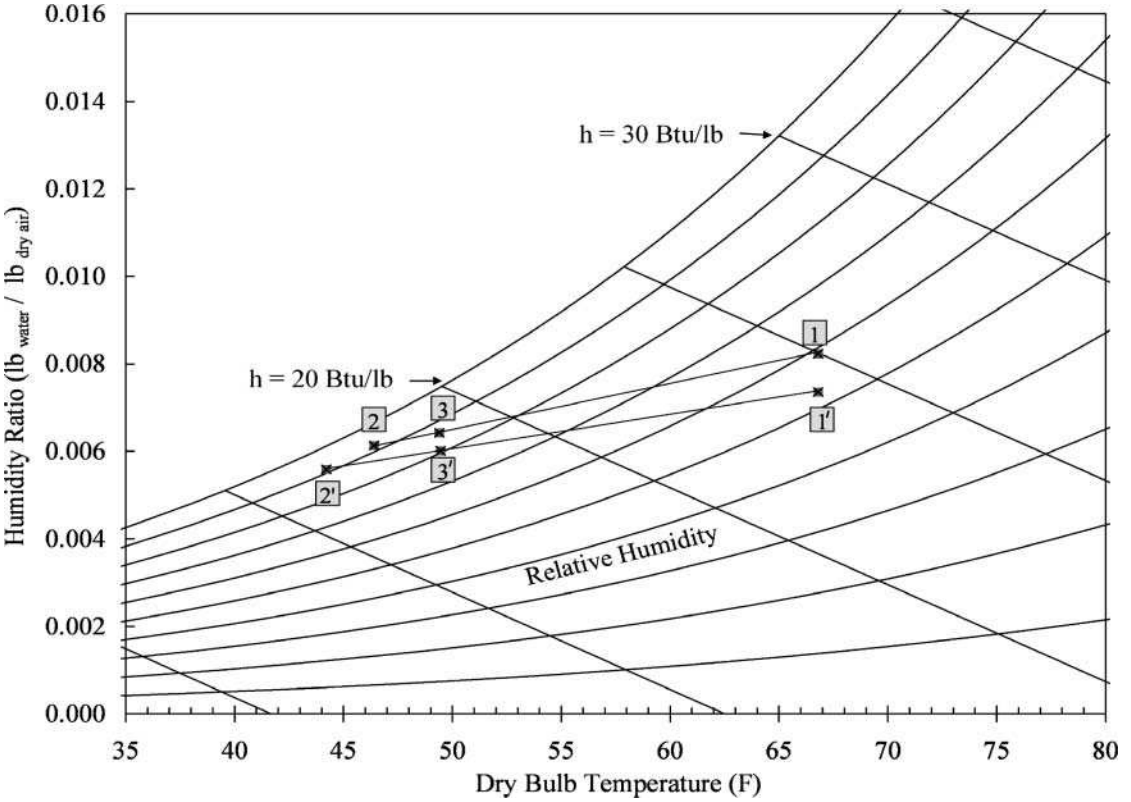

Figure 6. Psychrometric presentation of the process before and after blocking areas of air bypass.

Psychrometric analysis after sealing

State point 1 represents the return air conditions after sealing. At state point 1, temperature and relative humidity of the air were 66.810°F (19.339°C) and 59.000%, respectively, with a corresponding humidity ratio W_{in} = 0.008234 $lb_{water}/lb_{dry\text{-}air}$ ($kg_{water}/kg_{dry\text{-}air}$) and total enthalpy of return air of 25.139 Btu/lb (58.473 kJ/kg). State point 2 shows the properties of the air leaving the indoor coil. The temperature and the relative humidity were 46.197°F (7.887°C) and 92.200%, respectively, with a corresponding humidity ratio W_C = 0.006132 $lb_{water}/lb_{dry\text{-}air}$ ($kg_{water}/kg_{dry\text{-}air}$). Total enthalpy associated to the air was 17.804 Btu/lb (41.412 kJ/kg). State point 3 represents the properties of the supply air. Temperature and relative humidity of the supply air were 49.380°F (9.656°C) and 86.290%, respectively. Humidity ratio W_{out} was 0.006427

Table 7. Efficiency of heat pump after sealing each step (site 5).

Order of sealing	Efficiency (EER)
1. Baseline measurement	11.373 ± 0.601
2. Holes at the top panel and the open cell foam gasket between the cabinet and the face panel	11.802 ± 0.651
3. Gaps around the edges of the front panel and bottom left corner	12.675 ± 0.662
4. Gaps around the indoor coil	12.946 ± 0.681
5. Pipe penetrations through the rear of the cabinet	13.008 ± 0.679

Table 8. Efficiency (COP) of heat pump in heating mode (site 5).

Test	Efficiency (COP)
1. Baseline measurement	2.554 ± 0.162
2. After all sealing	3.042 ± 0.191

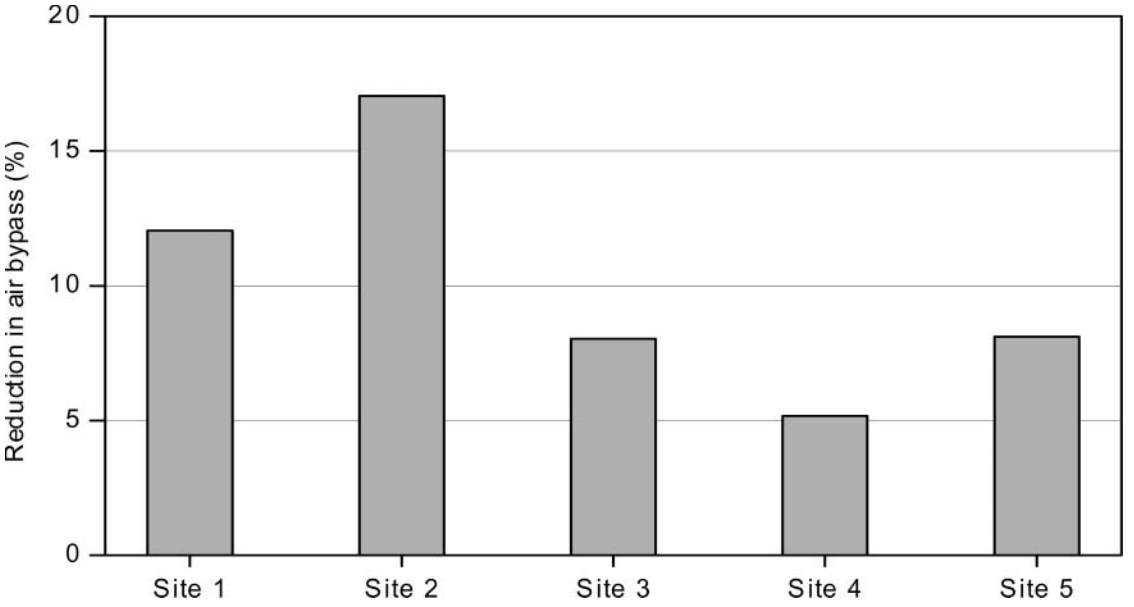

Figure 7. Reduction in air bypass after sealing accessible holes.

$lb_{water}/lb_{dry\text{-}air}$ ($kg_{water}/kg_{dry\text{-}air}$), and the enthalpy associated to the supply was 18.891 Btu/lb (43.940 kJ/kg).

After the sealing, the SHR decreased, the latent capacity of the unit increased, and the TCC increased. Further, as shown in the psychrometric chart (Figure 6), the temperature leaving the indoor coil after the sealing increased by 2.000°F (1.111°C); however, the supply air temperature did not change at all. This is due to the fact that when the air was bypassing the indoor coil, a fraction of the total return air was mixing with the air leaving the indoor coil. As a result, before blocking the areas of air bypass, the temperature of the air leaving the indoor coil was 2.000°F (1.111°C) lower than the air temperature leaving the coil after the sealing.

It is noted that the relative humidity in the room after air-sealing is approaching ~60%. This is likely due to the unusual low dry-bulb temperature (approximately 67°F [19.4°C]) during the tests. The reduction in air bypass to create a high-humidity situation is not anticipated in general.

Summary of the field test results

As mentioned above, heat pumps at five sites were tested. The results of all the sites are summarized in this section. Figure 7 shows the percentage reduction in air bypass obtained at all five sites. A ~5% to 17% reduction in air bypass after sealing all accessible locations of air bypass was obtained. Figure 8 shows the percentage improvements in cooling efficiency at all five sites chosen in this study. A ~7% to 17% improvement in the efficiency was obtained in the cooling mode, whereas a ~5% to 11% improvement was obtained in total cooling capacities (Figure 9). Similarly, tests in the heating mode were performed at sites 4 and 5, and results showed ~16% and 19% improvement in efficiency at site 4 and 5, respectively.

Though the heat pump units are primarily designed to either cool or heat the space, these units also dehumidify the air. The TCC comprises two separate components—the SCC, which is associated with lowering the dry-bulb temperature of the air, and the LCC, which is associated with removing moisture from the air. The SHR is the ratio of the SCC to TCC. The SHR of the heat humps typically vary between 0.682 to 0.798, which is necessary to maintain the humidity level in the space by continuously removing moisture from the air, because high humidity can cause discomfort, surface material deterioration, condensation, and corrosion. In this study, it was found that due to the air bypass problem, the SHR of the heat pumps increased. Figure 10 shows reduction (%) in SHR at each site after sealing. A 2.751% to 12.002% reduction in SHR was observed.

Table 9 shows the statistical analysis of air bypass at each site. It can be noted in Table 9 that all loca-

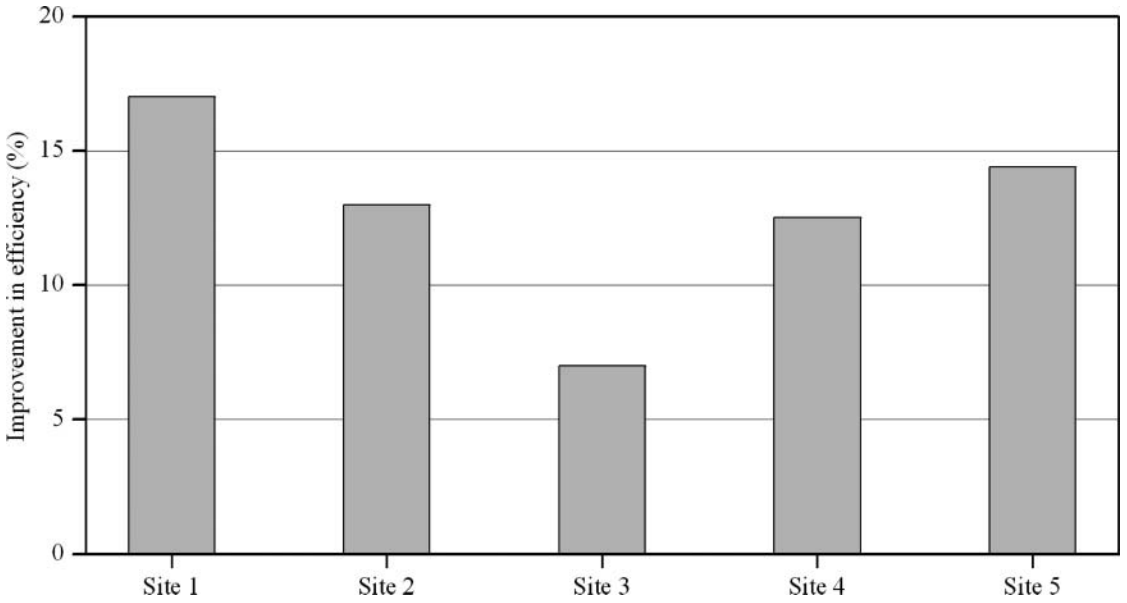

Figure 8. Improvement in efficiency (EER) when the heat pumps were running in cooling mode.

tions of air bypass could not be sealed. On average, 54.476% of air bypass was reduced. A significant amount of air was bypassing from other inaccessible holes. Using linear approximation, it is speculated that if the majority of bypass (including inaccessible hidden bypass) is reduced, the efficiency of the heat pumps might be improved as much as 25%.

As mentioned above, the air bypass locations can be divided into two types—locations that can be found only in VSWSHPs and locations that are common in all types of WSHPs. Table 10 shows that 44.889% of air was bypassing through gaps and holes that can be found only in VSWSHPs, and the rest (55.111%) of the air was bypassing

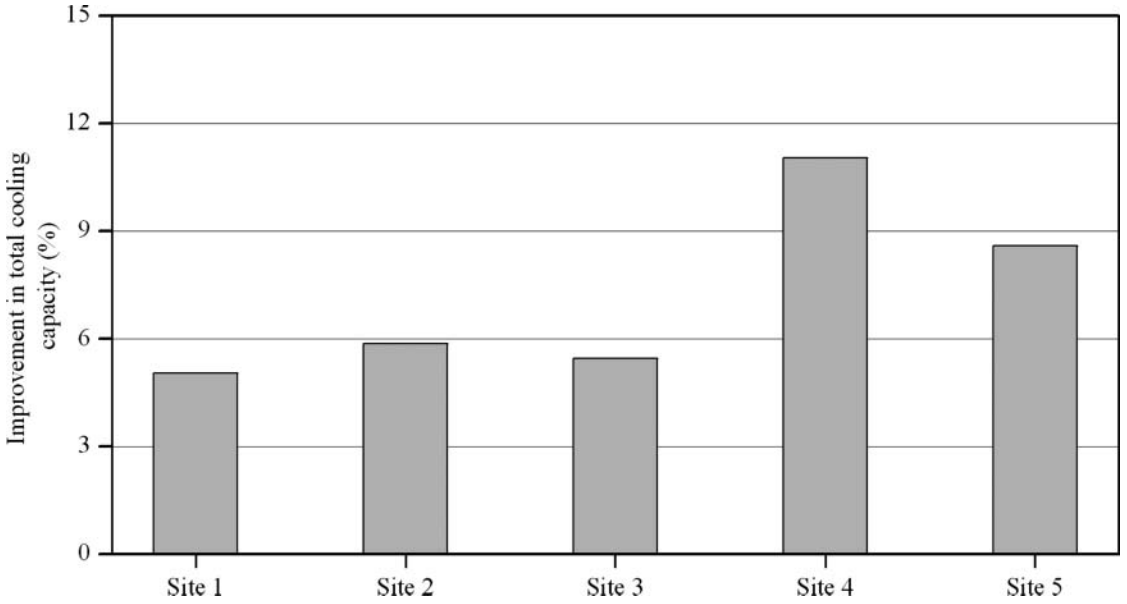

Figure 9. Improvement in TCC after blocking potential areas of air bypass.

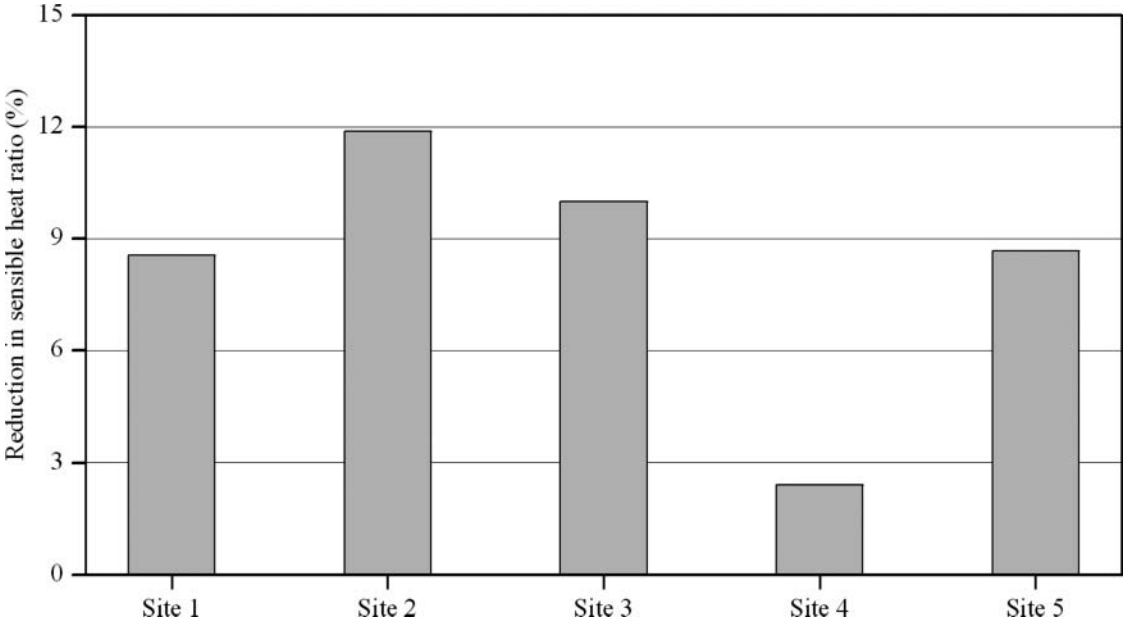

Figure 10. Reduction in SHR (SCC/TCC) after blocking potential areas of air bypass.

through locations that can be identified in any type of WSHP.

A natural question is "Who should seal the air bypass"? Most of the air bypass relates to the design of the heat pumps themselves, at sheet metal seams, control and electrical devices, etc. Some of the air bypass sites relate to the installation, for example, where the water pipes penetrate the cabinet. These penetrations need to allow pipe movement due to thermal expansion and contraction, so instructions from manufacturers typically call for the contractor to seal the penetrations. But the holes are large and have been found to consistently be sealed poorly. It is recommended that manufacturers use some form of flexible seal, such as a boot (similar to the seal on automobile stick-shifts), that provide air-sealing while allowing for pipe movement. Efficiency testing of heat pumps for ratings should require use of factory-shipped sealing of the heat pumps rather than simulation of what the installing contractor will do to air-seal the units.

Benefits of reducing air bypass

There are several energy benefits that can be derived from reducing air bypass. In both heating and cooling, the heat pump capacity drops due to air bypass, making the heat pump run longer and less efficiently. Further, in cooling, the indoor coil can freeze, leading to zero capacity by stopping or significantly reducing cool air output from the system. Environmental benefits result from reduced energy losses. Indoor comfort will be improved where air

Table 9. Analysis of air bypass at each site.

Location	Air bypass before sealing,%	Air bypass after sealing,%	Reduction in air bypass,%	Improvement in EER,%
Site 1	29.204	17.102	12.087	16.993
Site 2	23.003	7.094	16.904	13.003
Site 3	15.295	7.277	8.012	6.931
Site 4	17.122	12.042	5.105	12.505
Site 5	24.022	15.608	8.105	14.411
Average	21.729	11.825	10.043	12.769

Table 10. Percentage distribution of air bypass associated with the types of locations in VSWSHP.

Types of locations	Type 1	Type 2
Percent distribution	44.889	55.111

bypass problems are so severe that heat pumps cannot meet the building heating and cooling loads. In addition, better dehumidification will also improve indoor air quality. Reduced energy losses will result in reduced costs in buildings where heat pump air bypass is eliminated.

Conclusion

The study investigates the air bypass problem in VSWSHPs. It is shown that air bypass can significantly increase VSWSHP energy usage. Blocking areas of air bypass in heat pumps in both cooling and heating modes seems to be a direct and attractive approach and can lead to energy savings. In this article, three methods are proposed to detect and diagnose the air-bypass problem. Five sites were selected for testing where VSWSHPs were installed and used to provide both heating and cooling to designated areas of the buildings. Several different air-bypass routes were found, each of which contributed significantly to the problem. It is also shown that the air bypass problem caused performance degradation of the heat pump in both cooling as well in heating. The test results showed ~5% to 11% improvement in TCC, ~7% to 17% improvement in cooling efficiency (EER), and ~16% to 19% improvement in heating efficiency (COP) of VSWSHPs compared to the baseline system when air bypass areas were sealed. Of the three methods tested, the balometer method appears to be the most accurate, while the blocked-coil method might be the most useful for commissioning and diagnostic tests.

Acknowledgment

The support of New York State Energy Research and Development Authority (NYSERDA) under agreement number 10902 is gratefully acknowledged.

Nomenclature

c_{pa} = specific heat of moist air, Btu/lb-°F (kJ/kg-°C)
$e_{X\text{-}1,\ldots,J}$ = uncertainty in the variables $X_{1,\ldots,J}$
e_Y = overall uncertainty
h_b = enthalpy of bypass air, Btu/lb (kJ/kg)
h_c = enthalpy of air leaving the coil, Btu/lb (kJ/kg)
h_{in} = enthalpy of the return air, Btu/lb (kJ/kg)
h_m = enthalpy of air leaving the heat pump, Btu/lb (kJ/kg)
h_{out} = enthalpy of the supply air, Btu/lb (kJ/kg)
m_b = mass flow of bypass air, lb (kg)
m_c = mass flow of air passing through the coil, lb (kg)
m_m = mass flow of air leaving the heat pump, lb (kg)
m_{out} = mass flow of air leaving the heat pump, lb (kg)
P_{hp} = instantaneous heat pump power, Btu/hr (kW)
RH_{in} = return air relative humidity
RH_{out} = supply air relative humidity
T_C = air temperature leaving the indoor coil, °F (°C)
T_{in} = return air temperature, °F (°C)
T_{out} = supply air temperature, °F (°C)
V = volumetric flow rate, ft^3/min (m^3/min)
W_{in} = specific humidity of the return air, lb/lb (kg/kg)
W_{out} = specific humidity of the supply air, lb/lb (kg/kg)
$X_{1,\ldots,J}$ = number of variables in uncertainty analysis
v = specific volume of the supply air, ft^3/lb (m^3/kg)

Abbreviations

COP = coefficient of performance of heat pump
EER = energy efficiency ratio of heat pump, Btu/hr per watt (W/W)
EWB = entering wet-bulb temperature, °F (°C)
EWT = entering water temperature, °F (°C)
LCC = latent cooling capacity, Btu/hr (kJ/hr)
SCC = sensible cooling capacity, Btu/hr (kJ/hr)
SHR = sensible heat ratio
TCC = total cooling capacity, Btu/hr (kJ/hr)
THC = total heating capacity, Btu/hr (kJ/hr)
VSWSHP = vertical stack water source heat pump
WSHP = water source heat pump

References

ASHRAE. 2003 . DOE plan projects savings for new building energy costs. *ASHRAE Transactions* 6:65–66.

Dexter, A.L., and M. Benouarets. 1996. A generic approach to identifying faults in HVAC plants. *ASHRAE Transactions* 102(1):550–6.

Dexter, A.L., and D. Ngo. 2001. Fault diagnosis in air-conditioning systems: A multi-step fuzzy model-based approach. *HVAC&R Research* 7(1):83–102.

Diaz, G., M. Sen, K.T. Yang, and R.L. McClain. 2001. Adaptive neurocontrol of heat exchangers. *ASME Journal of Heat Transfer* 123(3):556–62.

DOE. 2003. *Buildings Energy Data Book*, Chapters 1 and 5. Washington, DC: U.S. Department of Energy.

Downey, T., and J. Proctor. 2002. What can 13,000 air conditioners tell us? *Proceedings of the ACEEE Summer Study on Energy Efficiency in Buildings* 1:52–67.

Grimmelius, H.T., J.K. Woud, and G. Been. 1995. On-line failure diagnosis for compression refrigerant plants. *International Journal of Refrigeration* 18(1):31–41.

Holman, J.P. 2001. *Experimental Methods for Engineers, 7th ed.*, pp. 48–143. New York: McGraw-Hill.

Katipamula, S., and M.R. Brambley. 2005a. Methods for fault detection, diagnostics and prognostics for building systems—a review, Part I. *HVAC&R Research* 11(1):3–25.

Katipamula, S., and M.R. Brambley. 2005b. Methods for fault detection, diagnostics and prognostics for building systems—a review, Part II. *HVAC&R Research* 12(2):169–87.

Kelso, R.M., and J.A. Wright. 2005. Application of fault detection and diagnosis techniques to automated functional testings. *ASHRAE Transactions* 111(1):964–70.

Lee, W.Y., M. House, and N.H. Kyong. 2005. Sub-system level fault diagnosis of a building's air-handling unit using general regression neural networks. *Applied Energy* 77(2):153–70.

Li, H., and J.E. Braun. 2003. An improved method for fault detection and diagnosis applied to package air conditioners. *ASHRAE Transactions* 109(2):683–92.

Navarro-Esbri, J.E. Torrella, and R. Cabello. 2007. A vapor compression chiller fault detection technique based on adaptive algorithms: Application to on-line refrigerant leakage detection. *International Journal of Refrigeration* 29(5):716–23.

Proctor, J. 2004. Residential and small commercial central air conditioning: Rated efficiency isn't automatic. *ASHRAE Winter Meeting, Anaheim, CA*, January 26 (presentation at the public session).

Reddy, T.A. 2007. Application of a generic evaluation methodology to assess four diffeerent chiller FDD methods. *HVAC & R Research* 13(5):711–29.

Rossi, T.M. 2004. Unitary air conditioner field performance. *International Refrigeration and Air Conditioning Conference, West Lafayette, IN*, July 12–15, Paper No. R146.

U.S. Census Bureau. 2006. Refrigeration, air-conditioning, and warm air heating equipment. Report MA333M 06 (1). Washington, DC.

Varshney, K., and P.K. Panigrahi. 2005. Artificial neural network control of a heat exchanger in a closed flow air circuit. *Applied Soft Computing* 5(4):441–65.

Walker, I., J. Siegel, K. Brown, and M. Sherman. 1998. Saving tons at the register. *Proceedings of the 1998 ACEEE Summer Study on Energy Efficiency in Buildings* 1:367–84.

Wang, S.W., and J.B. Wang. 1999. Law-based sensor fault diagnosis and validation for building air-conditioning systems. *HVAC&R Research* 5(4):353–78.

Wang, S.W., and F. Xiao. 2004. AHU sensor fault diagnosis using principal-component analysis method. *Energy and Buildings* 36(2):147–60.

Appendix

This appendix provides the derivation of Equation 1. The conservation of energy at the point of mixing of bypass air and air leaving the coil is as follows:

$$m_b \times h_b + m_c \times h_c = m_m \times h_m.$$

It is assumed that supply air leaving the unit is at the same condition as the mixed air, neglecting the fan motor heat, and making another simplifying assumption that there is no leakage between the mixed air point and the supply air point:

$$m_{out} \times h_{out} = m_m \times h_m.$$

The simplifying assumption is then made that the bypass air is at the condition of the return air. This is mostly the case, although in some instances, air leaking from behind the heat pump may be at slightly different conditions. Rearranging:

$$m_b \times h_{in} + m_c \times h_c = m_{out} \times h_{out}.$$

By conservation of mass at the point of mixing of bypass air:

$$m_b + m_c = m_m.$$

Using the assumption that there is no leakage through the fan and supply section:

$$m_b + m_c = m_{out}.$$

Rearranging:

$$m_b \times h_{in} + m_c \times h_c = m_b \times h_{out} + m_c \times h_{out}$$

Further rearranging:

$$m_b \times (h_{in} - h_{out}) = m_c \times (h_{out} - h_c).$$

For the heat pump operating in heating mode, or in cooling mode if latent heat is neglected, changes in enthalpy can be simplified to

$$h_{in} - h_{out} = c_{pa} \times (T_{in} - T_{out}).$$

and

$$h_{out} - h_c = c_{pa} \times (T_{out} - T_c).$$

The air-bypass is defined as:

$$\text{Air-bypass} = \frac{m_b}{m_{out}}.$$

where m_{out} is used as the total airflow. Rearranging:

$$\text{Air-bypass} = \frac{m_b}{m_b + m_c}.$$

From above:

$$m_b = \frac{m_c \times (h_{out} - h_c)}{h_{in} - h_{out}}.$$

so

$$\text{Air-bypass} = \frac{\left[\frac{m_c \times (h_{out} - h_c)}{h_{in} - h_{out}}\right]}{\left[\frac{m_c \times (h_{out} - h_c)}{h_{in} - h_{out}}\right] + m_c}.$$

or

$$\text{Air-bypass} = \frac{\left[\frac{(T_{out} - T_c)}{T_{in} - T_{out}}\right]}{\left[\frac{(T_{out} - T_c)}{T_{in} - T_{out}}\right] + 1}$$

This simplifies to

$$\text{Air-bypass} = \frac{(T_{\text{out}} - T_c)}{(T_{\text{in}} - T_c)}$$